Effects of microwave and oxygen plasma treatments on capacitive characteristics of supercapacitor based on multiwalled carbon nanotubes

2016 Jpn. J. Appl. Phys. 55 02BD05

(http://iopscience.iop.org/1347-4065/55/2S/02BD05)

Japanese Journal of Applied Physics **55**, 02BD05 (2016)
http://doi.org/10.7567/JJAP.55.02BD05

REGULAR PAPER

Effects of microwave and oxygen plasma treatments on capacitive characteristics of supercapacitor based on multiwalled carbon nanotubes

Paweena Dulyaseree[1], Visittapong Yordsri[2], and Winadda Wongwiriyapan[1,3,4*]

[1]*College of Nanotechnology, King Mongkut's Institute of Technology Ladkrabang, Bangkok 10520, Thailand*
[2]*National Metal and Materials Technology Center, Pathunthani 12120, Thailand*
[3]*Nanotec-KMITL Center of Excellence on Nanoelectronics Device, Bangkok 10520, Thailand*
[4]*Thailand Center of Excellence in Physics, CHE, Bangkok 10400, Thailand*

*E-mail: kwwinadd@kmitl.ac.th

Received July 1, 2015; accepted October 7, 2015; published online January 26, 2016

The effects of microwave and oxygen plasma treatments on the capacitive characteristics of a supercapacitor based on multiwalled carbon nanotubes (MWNTs) were investigated. MWNTs were heat-treated under air ambient at 500 °C for 1 h, and subsequently microwave-treated at 650 W for 70 s (m-MWNTs). Another batch of MWNTs was treated by oxygen plasma for 30 min (p-MWNTs). Pristine MWNTs, m-MWNTs, and p-MWNTs were separately used as electrode materials for supercapacitors. Their cyclic voltammetry, galvanostatic charge/discharge, and electrochemical impedance spectroscopy results were analyzed. The p-MWNTs show the best performance with a specific capacitance of 238.23 $F \cdot g^{-1}$. The capacitance improvement is attributed to the increase in the number of oxygen-containing functional groups, as evidenced by Fourier transform-infrared spectroscopy and contact angle measurement. These results suggest that oxygen plasma treatment is a rapid and efficient method for oxygen functionalization.

1. Introduction

A supercapacitor, also called an electrochemical capacitor, is a kind of electrical device for energy storage, bridging the gap between batteries and dielectric capacitors. Supercapacitors have gained considerable attention in recent years as an energy storage device owing to their high power density, high rates of charge/discharge, and long cycle life.[1–5] Supercapacitors are classified as electrical double-layer capacitors (EDLCs) and pseudocapacitors according to charge storage mechanisms.[3] The typical electrode materials of EDLCs are carbon materials with a high surface area, which can store energy in the double layers on the surface of carbon materials.[6] In the case of pseudocapacitors, the most commonly used electrode materials are metal oxides and conducing polymers, which can transfer the faradaic charges between an electrode and an electrolyte.[7]

An EDLC consists of three important parts: an electrode, a separator, and an electrolyte. To improve the performance of EDLCs, most efforts have been focused on the improvement of electrode materials. Electrode materials are required to have high specific surface area, good conductivity, and good chemical stability properties.[8,9] Various different carbon forms can be used as materials in an EDLC electrode such as activated carbon, carbon aerogels, carbon nanotubes (multi- and single-walled carbon nanotubes), and graphene.[10] An EDLC based on carbon nanotube materials exhibited good electrical performance.[11] Recently, substantial efforts have been expended to improving the electrochemical performance of carbon-based electrodes through modifying the surface of carbon materials by, for example, functionalization with various metal oxides or a conductive polymer, or by treatment with plasma.[12–20] Functionalization of the electrode material surface with oxygen-containing functional groups is key to the enhancement of supercapacitor performance.[21–26] Since the pristine carbon surface is hydrophobic, the high resistance between the carbon surface and the aqueous electrolyte hinders the accessibility of the electrolyte ions into the carbon materials.[15,26,27]

In this study, we tailored the carbon-based materials by surface modification using low-cost equipment with rapid time and efficiency. The multiwalled carbon nanotube (MWNT) functionalization by microwave treatment using a commercial microwave oven and oxygen plasma treatment using a commercial oxygen plasma cleaner were investigated. The electrochemical characteristics of the surface-modified MWNTs were evaluated.

2. Experimental methods

Three types of MWNT-based electrodes were prepared: pristine MWNTs, microwave-treated MWNTs (m-MWNTs), and plasma-treated MWNTs (p-MWNTs). For microwave treatment, 2.5 g of MWNTs (diameter, 10–20 nm; length, 1–5 μm) was treated by heating under air ambient at 500 °C for 1 h and subsequently treated with microwave in air at 650 W for 70 s (hereinafter referred to as m-MWNTs) using a commercial microwave oven. For plasma treatment, 0.55 g of MWNTs was treated with oxygen plasma using an expanded plasma cleaner (Harrick Scientific) at an RF frequency of 13.56 MHz and a power of 18 W for 30 min (hereinafter referred to as p-MWNTs). Next, the MWNT paste was prepared by mixing the treated MWNTs and poly(vinylidene fluoride) (PVDF) at a weight ratio of 11 : 1 in *n*-methyl-2-pyrrolidone (NMP) using a homogenizer at 7,000 rpm for 30 min and subsequently sonicated in an ultrasonic bath for 30 min. To fabricate MWNT-based electrodes for a supercapacitor, stainless-steel-type 304 (SS304) was used as a current collector. SS304 was cleaned by soaking in 37% hydrochloric acid (HCl) for 10 min and washed with deionized water to remove residual HCl solution until its pH became neutral. The prepared MWNT paste was dip-coated on the treated SS304 with an area of $5 \times 5\,mm^2$ and dried at room temperature overnight. The weight of the treated MWNT coating on SS304 was measured by weighing the SS304 before and after coating using a digital balance. The treated MWNTs were characterized in terms of their functional groups and structures by Fourier transform-infrared spectroscopy (FT-IR; Thermo Scientific Nicolet

6700), Raman spectroscopy (Thermo Scientific DXR Smart Raman), and transmission electron microscopy (TEM; JEOL JEM-2010). The hydrophilicity property of the treated MWNTs was characterized by the contact angle technique (Dataphysics OCA 40). A droplet of 1 M Na_2SO_4 aqueous solution (a volume of 1 µl) was dropped on the treated-MWNT-coated SS304.

Electrochemical measurements of the treated MWNTs were carried out in a three-electrode cell connected to an electrochemical workstation (Metrohm AUTOLAB PGSTAT 302). The treated-MWNT-based SS304 was used as a working electrode. The Pt and Ag/AgCl electrodes were used as the counting and reference electrodes, respectively. 1 M Na_2SO_4 aqueous solution was used as the electrolyte. Electrochemical properties were characterized by cyclic voltammetry (CV), galvanostatic charge/discharge (CD), and electrochemical impedance spectroscopy (EIS) techniques. CV tests were operated in a potential range of 0.0 to 0.8 V at scan rates of 5 and 100 $mV \cdot s^{-1}$. CD tests were carried out in a potential range of −0.2 to 1.0 V at a constant current of 1 mA. EIS was carried out in a frequency range between 10 kHz and 0.01 Hz at an amplitude of 5 mV. The specific capacitances of the supercapacitor (C_S) were evaluated from CV and CD curves using the following equations:

$$C_S = \frac{\int_{V_1}^{V_2} i(V)\,dV}{2(V_2 - V_1)mv}, \quad (1)$$

$$C_S = \frac{I \times \Delta t}{\Delta V \times m}, \quad (2)$$

where $\int_{V_1}^{V_2} i(V)\,dV$ is the total voltammetric charge obtained by the integration of positive and negative sweeps in the CV curve, $V_2 - V_1$ is the potential window width (V), m is the weight of the treated MWNTs in the electrode paste (g), v is the scan rate ($V \cdot s^{-1}$), I is the discharge current (A), Δt is the discharge time (s), and ΔV represents the voltage change after a full charge or discharge (V).

3. Results and discussion

The changes in surface functional groups of pristine MWNTs after microwave and oxygen plasma treatments were confirmed from FTIR spectra through the changes in peak positions as well as the appearance of new peaks. Figure 1(a) shows comparative FT-IR spectra of the pristine MWNTs, m-MWNTs, and p-MWNTs with several peaks of functional groups. The broad peak at 3432 cm^{-1} corresponds to the stretching vibration of the hydroxyl group (–OH). The bands at 2922 and 2856 cm^{-1} are attributed to the C–H stretching vibrations of the methyl group. The peak at 2360 cm^{-1} could be assigned to CO_2 that was absorbed during the FTIR spectra measurements. The absorption bands at 1750, 1640, and 1596 cm^{-1} are assigned to the stretching vibrations of the carboxyl, carbonyl (C=O), and aromatic rings (C=C), respectively.[28] The band at 1020 cm^{-1} is assigned to the stretching vibration of the C–O group. Moreover, the new peaks at 3742 cm^{-1} corresponding to the –OH stretching of the hydroxyl group apparently appeared from p-MWNTs, while a small peak appeared for the m-MWNTs. Interestingly, focusing at the peaks at 1640 and 1596 cm^{-1}, the aromatic ring stretching was largely suppressed and the carbonyl stretching was enhanced in the m-MWNTs and p-MWNTs. These results indicate that oxygen plasma and microwave treatments are effective methods for functionalizing oxygen-containing functional groups on the walls of MWNTs. However, the chemical bonds between oxygen and carbon on the MWNT sidewall require further confirmation by X-ray photoelectron spectroscopy.

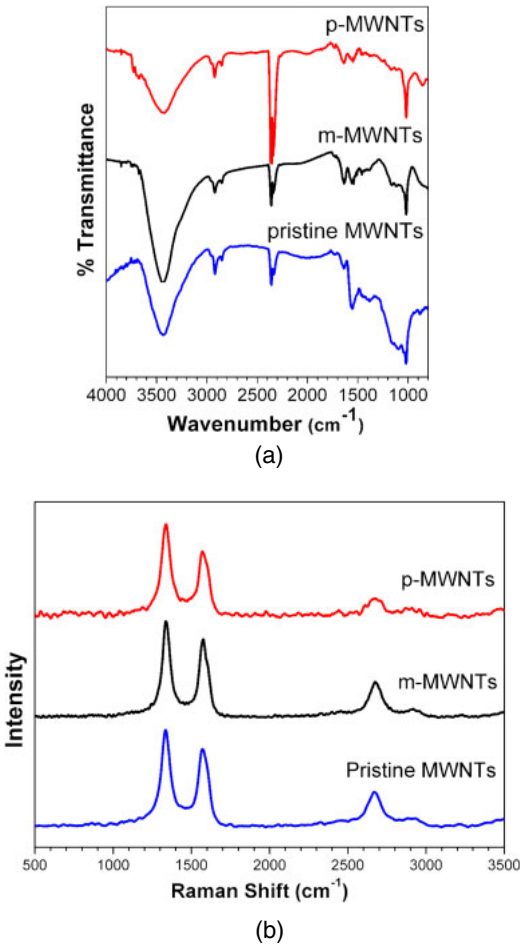

Fig. 1. (Color online) (a) FT-IR and (b) Raman spectra of the different electrode materials.

The purity and crystallinity of MWNTs were characterized by Raman spectroscopy using an argon ion laser with a wavelength of 532 nm (2.33 eV) as an excitation light at a power of 5 mW. As shown in Fig. 1(b), the Raman spectra of pristine MWNTs, m-MWNTs, and p-MWNTs consist of two characteristic peaks, which are the so-called D-band, which originated from the disordered carbon structure and sp^3 hybridized carbon at a Raman shift of ~1336 cm^{-1}, and the G-band, which originated from the graphitic structure dominated by sp^2 bonds at a Raman shift of ~1567 cm^{-1}.[29,30] Generally, the purity and crystallinity of MWNTs can be evaluated on the basis of the I_D/I_G ratio between the intensities of D and G bands. An increase in I_D/I_G ratio indicates the impurity structure and a higher proportion of sp^3 carbon.[30,31] It is found that the I_D/I_G ratio increased after MWNT treatments, i.e., the I_D/I_G ratios were 1.22, 1.26, and 1.41 for pristine MWNTs, m-MWNTs, and p-MWNTs, respectively. This result implies that oxygen plasma could etch sp^2 carbon faster than sp^3 carbon.[19]

The nanostructure of MWNTs was investigated by TEM. Figures 2(a)–2(c) show TEM images of pristine MWNTs,

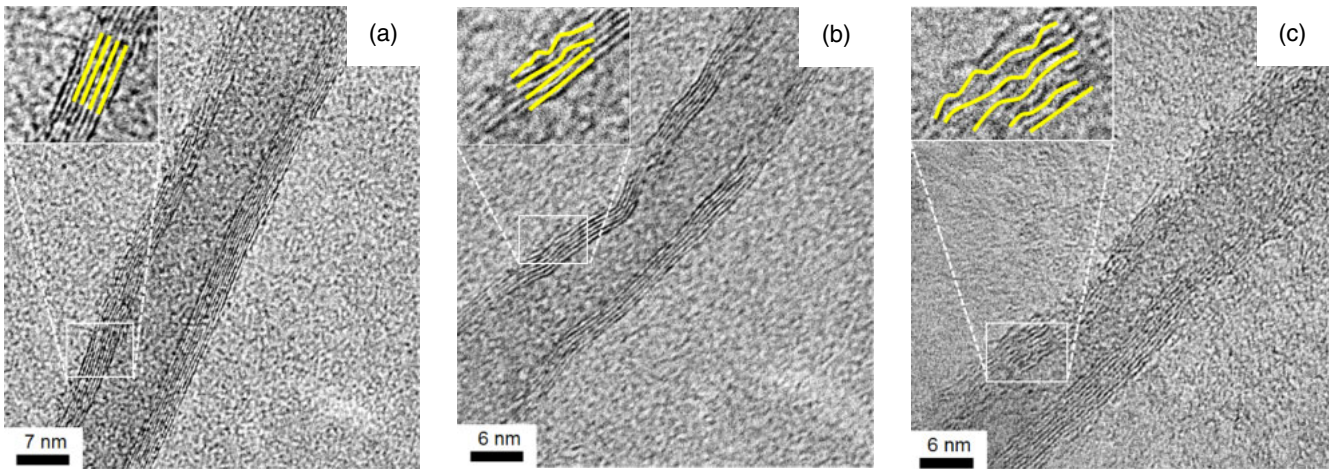

Fig. 2. (Color online) TEM images of (a) pristine MWNTs, (b) m-MWNTs, and (c) p-MWNTs.

m-MWNTs, and p-MWNTs, respectively. Figure 2(a) shows graphene planes parallel to each other and parallel to the axis of the tubular structure, implying an MWNT structure, illustrating as straight lines in the inset. As can be observed in Fig. 2(b), the m-MWNTs had partly damaged sidewalls, illustrated as curved lines in the inset. The damage on sidewalls was significantly increased in p-MWNTs [see Fig. 2(c)]. However, it was found that only the outer walls of MWNTs were damaged owing to defect generation, while the inner walls of MWNTs still remained intact. The TEM results coincided with the I_D/I_G of Raman spectra, which indicates the purity and crystallinity of MWNTs.

Next, the contact angle (CA) measurements were conducted to characterize the wettability of the substrate. CA can define the wettability degree, on the basis of which the surface is classified as superhydrophilic (CA < 5°), hydrophilic (CA < 90°), hydrophobic (CA > 90°), or superhydrophobic (CA > 150°).[32] Figures 3(a)–3(c) show the droplet of 1 μL of 1 M Na_2SO_4 aqueous solution on pristine-MWNT-, m-MWNT-, and p-MWNT-coated SS304 substrates, respectively. The contact angles of the pristine MWNTs, m-MWNTs and p-MWNTs are approximately 113.84 ± 4.15, 36.48 ± 8.69, and $19.87 \pm 5.05°$, respectively. The p-MWNTs show low contact angles, implying the best hydrophilicity property. The improved wettability of the p-MWNT-coated SS304 was attributed to the oxygenated functional group functionalization and the surface roughness of MWNTs owing to the defects as evidenced by FT-IR and TEM results.

Figure 4(a) shows CV curves of pristine MWNTs, m-MWNTs, and p-MWNTs in a potential window of 0 to 0.8 V at a scan rate of 100 $mV \cdot s^{-1}$. The CV curves showed typical EDLC characteristics and are rectangular with no obvious redox peak. The clear rectangular curves further reflect a higher ion diffusion rate in the electrode materials. From the area of the CV curve, the specific capacitances were calculated using Eq. (1). The specified capacitances of the pristine MWNTs, m-MWNTs, and p-MWNTs were 61.46, 214.45, and 238.23 $F \cdot g^{-1}$, respectively. The p-MWNTs show the highest specific capacitance. Generally, pristine MWNTs are hydrophobic materials due to the sp^2 lattice of graphitic carbon. In the case of using pristine MWNTs as the electrode material in an aqueous electrolyte system, the high resistance

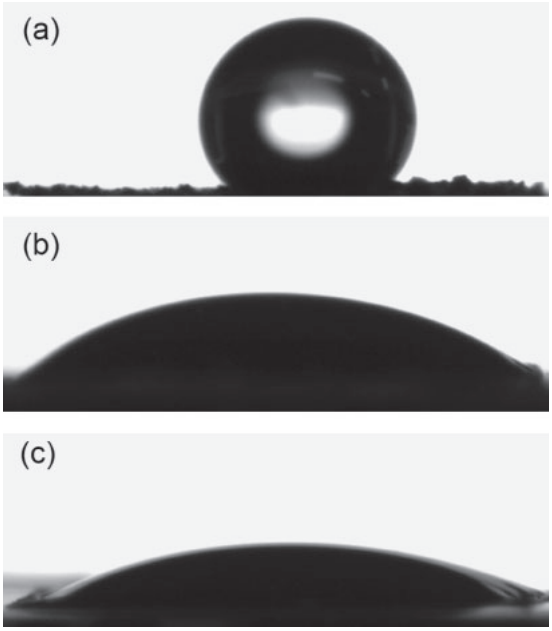

Fig. 3. Contact angles of (a) pristine MWNTs, (b) m-MWNTs, and (c) p-MWNTs.

between the carbon surface and the aqueous electrolyte hinders the accessibility of the electrolyte ions into the electrode materials. In this study, microwave and oxygen plasma treatments facilitate the easy control of the wetting properties of m-MWNTs and p-MWNTs as evidenced by the decrease in contact angle. Thus, the m-MWNTs and p-MWNTs allow electrolyte ions to access to their surface more easily than the pristine-MWNTs, resulting in an increase in capacitance.[15,33] Figure 4(b) shows the galvanostatic charge–discharge (CD) curves within the operating voltage range of −0.2 to 1 V at a current of 1 mA. The CD profiles show a shape of a nearly isosceles triangle, suggesting good electrochemical reversibility. No obvious voltage drop was observed at the discharge current, indicating a low internal resistance of the electrode.[34]

The resistance and capacitance of supercapacitors can be further explained by electrochemical impedance spectroscopy (EIS). EIS is a technique that can reveal the complex phenomena of electron interception and diffusion at the

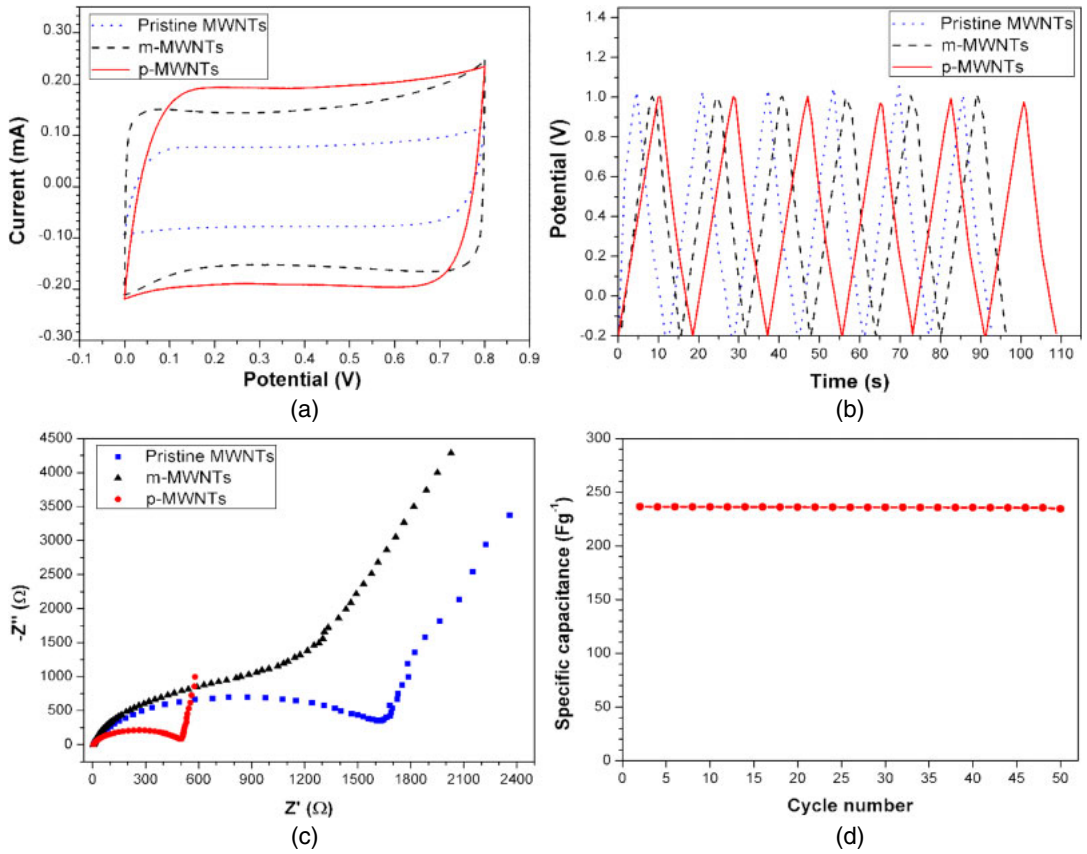

Fig. 4. (Color online) Electrochemical properties of different electrode materials in 1 M Na_2SO_4 aqueous electrolyte. (a) CV at a scan rate of 0.1 $V \cdot s^{-1}$, (b) galvanostatic charge/discharge curves at an applied constant current of 1 mA, (c) Nyquist plot in the frequency range of 10 kHz–0.01 Hz at an amplitude of 5 mV, and (d) cycling stability of p-MWNTs.

electrode–electrolyte interface. Figure 4(c) shows the Nyquist plots of the pristine MWNTs, m-MWNTs, and p-MWNTs in the frequency range of 10 kHz–0.01 Hz. The obtained Nyquist spectra for all the configurations consist of a semicircle in the high-frequency region, followed by a linear portion extending in the low-frequency regions. The slopes of the lines in the low-frequency regions ranging from highest to lowest correspond to the p-MWNTs, m-MWNTs, and pristine MWNTs, respectively. The p-MWNTs show a straight line with a slope near unity, indicating the highest ion diffusion rate at the interface between the electrolyte and electrode materials, and suggesting an ideal supercapacitive behavior. This high ion diffusion rate could be attributed to the wettability improvement of the electrode surface by the functionalization of the oxygen-containing functional group by plasma treatment.[18] The wettability of the electrode promotes the movement of Na^+ and SO_4^{2-} in the electrolyte penetrating deeply inside the micropores. The microwave-treated sample (m-MWNTs) shows a slight improvement in wettability.

The offset on the x-axis, Z' (Ω), of the high-frequency semicircle [see Fig. 4(c)] is a dominant resistive nature of the supercapacitor consisting of (i) electrolyte resistance, (ii) the intrinsic resistance of the electrode material, and (iii) the contact resistance between the electrode material and the current collector, which is a measure of series resistance, R_S.[35] The R_S values of the pristine MWNTs, m-MWNTs, and p-MWNTs are determined to be 4.99, 4.87, and 4.18 Ω, respectively. Since the same electrolyte, 1 M Na_2SO_4, was used in the EIS measurement, a decrease in the R_S of the treated MWNTs may be attributed to a decrease in the intrinsic resistance of the treated MWNTs due to the formation of intershell cross-linking by the oxygen-containing functional group,[36,37] and a decrease in contact resistance between the electrode material and the current collector due to the improvement of the wettability property.

The diameter of the semicircle represents the kinetic resistance to the charge transfer, called the charge transfer resistance (R_{CT}). The p-MWNTs show the smallest semicircle, implying the smallest R_{CT}, while the pristine MWNTs show the largest semicircle and thus the highest R_{CT}. This result indicates the good charge transfer in the electrolyte–electrode interface, which is due to the improvements in the conductivity and wettability of the treated MWNTs. Note that the EIS-measured impedance included contributions from both the MWNT-based electrodes and the electrolyte. The supercapacitor fabrication process was kept the same; only the MWNTs differed owing to the treatment process. Therefore, the measured Re(Z) values reflected the effects of only the properties and morphologies of the treated MWNTs.

Figure 4(d) shows the specific performance vs the number of CV cycles for the p-MWNT-based supercapacitor. The specific capacitance of p-MWNTs changes from 236.63 to 234.57 $F \cdot g^{-1}$ (remains 99.13%) after 50 cycles at the scan rate of 100 $mV \cdot s^{-1}$. Although the p-MWNTs may seem to deteriorate easily, they still show good stability with good retention of capacitance, showing a promising use as energy storage devices.

4. Conclusions

The effects of microwave and oxygen plasma treatments on the capacitive characteristics of a supercapacitor based on MWNTs were investigated. FT-IR, Raman spectroscopy, TEM, and contact angle measurement indicated that the hydroxyl functional groups were introduced, the surface morphology of the MWNTs was changed, and the wettability property was improved after oxygen plasma treatment. The electrochemical measurement reveals that MWNTs modified by oxygen plasma show the highest specific capacitance of $238.23\,\mathrm{F{\cdot}g^{-1}}$. Moreover, R_S is reduced to $4.18\,\Omega$ and the specific capacitance can be maintained at 99.13% after 50 cycles. The capacitance improvement is attributed to the increase in the number of oxygen-containing functional groups, suggesting that oxygen plasma treatment is a rapid and efficient method for the modification of MWNTs. These preliminary results suggest that the p-MWNTs are a promising electrode material for EDLC application.

Acknowledgments

We acknowledge the support from the KMITL Research Fund (KREF045508) and support from the National Nanotechnology Center (NANOTEC), NSTDA, Ministry of Science and Technology, Thailand, through its program of the Center of Excellence Network and the Thailand Center of Excellence in Physics (ThEP). P.D. acknowledges the support from the Office of the Higher Education Commission (OHEC).

1) C. Arbizzani, M. Mastragostino, and F. Soavi, J. Power Sources **100**, 164 (2001).
2) J. R. Miller and P. Simon, Science **321**, 651 (2008).
3) R. Kötz and M. Carlen, Electrochim. Acta **45**, 2483 (2000).
4) A. Burke, Electrochim. Acta **53**, 1083 (2007).
5) P. Simon and Y. Gogotsi, Nat. Mater. **7**, 845 (2008).
6) A. G. Pandolfo and A. F. Hollenkamp, J. Power Sources **157**, 11 (2006).
7) B. E. Conway, V. Birss, and J. Wojtowicz, J. Power Sources **66**, 1 (1997).
8) J. R. Miller, R. A. Outlaw, and B. C. Holloway, Science **329**, 1637 (2010).
9) Y. Zhu, S. Murali, M. D. Stoller, K. J. Ganesh, W. Cai, P. J. Ferreira, A. Pirkle, R. M. Wallace, K. A. Cychosz, M. Thommes, D. Su, E. A. Stach, and R. S. Ruoff, Science **332**, 1537 (2011).
10) F. Beguin and E. Frackowiak, *Supercapacitors: Materials, Systems, and Applications* (Wiley-VCH, Weinheim, 2013) p. 135.
11) Y. Zhai, Y. Dou, D. Zhao, P. F. Fulvio, R. T. Mayes, and S. Dai, Adv. Mater. **23**, 4828 (2011).
12) Y. Jin, H. Chen, M. Chen, N. Liu, and Q. Li, ACS Appl. Mater. Interfaces **5**, 3408 (2013).
13) L. Li, Z. A. Hu, N. An, Y. Y. Yang, Z. M. Li, and H. Y. Wu, J. Phys. Chem. C **118**, 22865 (2014).
14) C. C. Wang and C. C. Hu, Mater. Chem. Phys. **83**, 289 (2004).
15) J. H. Park, J. M. Ko, and O. O. Park, J. Electrochem. Soc. **150**, A864 (2003).
16) Q. Wu, Y. Xu, Z. Yao, A. Liu, and G. Shi, ACS Nano **4**, 1963 (2010).
17) C. C. Lai and C. T. Lo, RSC Adv. **5**, 38868 (2015).
18) K. Wang, C. Li, and B. Ji, J. Mater. Eng. Performance **23**, 588 (2014).
19) R. K. Gupta, M. Dubey, P. Kharel, Z. Gu, and Q. H. Fan, J. Power Sources **274**, 1300 (2015).
20) B. J. Yoon, S. H. Jeong, K. H. Lee, H. S. Kim, C. G. Park, and J. H. Han, Chem. Phys. Lett. **388**, 170 (2004).
21) R. L. McCreery, K. K. Cline, C. A. McDermott, and M. T. McDermott, Colloids Surf. **93**, 211 (1994).
22) E. Frackowiak, K. Metenier, V. Bertagna, and F. Beguin, Appl. Phys. Lett. **77**, 2421 (2000).
23) Y. T. Kim, Y. Ito, K. Tadai, T. Mitani, U. S. Kim, H. S. Kim, and B. W. Cho, Appl. Phys. Lett. **87**, 234106 (2005).
24) S. Ghosh, X. An, R. Shah, D. Rawat, B. Dave, S. Kar, and S. Talapatra, J. Phys. Chem. C **116**, 20688 (2012).
25) X. Xiao, T. Li, Z. Peng, H. Jin, Q. Zhong, Q. Hu, B. Yao, Q. Luo, C. Zhang, L. Gong, J. Chen, Y. Gogotsi, and J. Zhou, Nano Energy **6**, 1 (2014).
26) S. Deheryan, D. J. Cott, P. W. Mertens, M. Heyns, and P. M. Vereecken, Electrochim. Acta **132**, 574 (2014).
27) E. Dujardin, T. W. Ebbesen, H. Hiura, and K. Tanigaki, Science **265**, 1850 (1994).
28) Y. T. Kim and T. Mitani, J. Power Sources **158**, 1517 (2006).
29) M. S. Dresselhaus, G. Dresselhaus, R. Saito, and A. Jorio, Phys. Rep. **409**, 47 (2005).
30) M. S. Dresselhaus, A. Jorio, M. Hofmann, G. Dresselhaus, and R. Saito, Nano Lett. **10**, 751 (2010).
31) C. Chen, A. Ogino, X. Wang, and M. Nagatsu, Diamond Relat. Mater. **20**, 153 (2011).
32) A. O. Lobo, S. C. Ramos, E. F. Antunes, F. R. Marciano, V. J. Trava-Airoldi, and E. J. Corat, Mater. Lett. **70**, 89 (2012).
33) H. Zanin, E. Saito, H. J. Ceragioli, V. Baranauskas, and E. J. Corat, Mater. Res. Bull. **49**, 487 (2014).
34) D. P. Dubal, R. Holze, and P. Gomez-Romero, Sci. Rep. **4**, 7349 (2014).
35) B. Vidyadharan, I. I. Misnon, J. Ismail, M. M. Yusoff, and R. Jose, J. Alloys Compd. **633**, 22 (2015).
36) S. Agrawal, M. S. Raghuveer, H. Li, and G. Ramanath, Appl. Phys. Lett. **90**, 193104 (2007).
37) S. Lee and J. W. Peng, J. Phys. Chem. Solids **72**, 1101 (2011).